Available online at www.sciencedirect.com
ScienceDirect
Journal of Solid State Chemistry 180 (2007) 2429–2436
JOURNAL OF SOLID STATE CHEMISTRY
www.elsevier.com/locate/jssc

Contrasting oxide crystal chemistry of Nb and Ta: The structures of the hexagonal bronzes $BaTa_2O_6$ and $Ba_{0.93}Nb_{2.03}O_6$

W.Gus Mumme[a], Ian E. Grey[a,*], Robert S. Roth[b], Terrell A. Vanderah[b]

[a]*CSIRO Minerals, Box 312, Clayton South, Vic. 3169, Australia*
[b]*National Institute of Standards and Technology, Materials Science and Engineering Laboratory, Gaithersburg, MD 20899, USA*

Received 3 April 2007; received in revised form 30 May 2007; accepted 2 June 2007
Available online 26 June 2007

Abstract

The high-temperature hexagonal forms of $BaTa_2O_6$ and $Ba_{0.93}Nb_{2.03}O_6$ have *P6/mmm* symmetry with unit-cell parameters $a = 21.116(1)$ Å, $c = 3.9157(2)$ Å and $a = 21.0174(3)$ Å, $c = 3.9732(1)$ Å, respectively. Single crystal X-ray structure refinements for both phases are generally consistent with a previously proposed model, except for displacements of some Ba atoms from high-symmetry positions. The structures are based on a framework of corner- and edge-connected Nb/Ta-centred octahedra, with barium atoms occupying sites in four different types of [0 0 1] channels with hexagonal, triangular, rectangular and pentagonal cross-sections. The refinements showed that the non-stoichiometry in the niobate phase is due to barium atom vacancies in the pentagonal channels and to extra niobium atoms occupying interstitial sites with tri-capped trigonal prismatic coordination. The origin of the non-stoichiometry is attributed to minimisation of non-bonded Ba–Ba repulsions. The hexagonal structure is related to the structures of the low-temperature forms of $BaNb_2O_6$ and $BaTa_2O_6$, through a 30° rotation of the hexagonal rings of octahedra centred at the origin.

Keywords: Hexagonal $BaTa_2O_6$ structure; Hexagonal $Ba_{0.93}Nb_{2.03}O_6$ structure; Single-crystal refinements of hexagonal $BaTa_2O_6$ type

1. Introduction

In the active field of research on photocatalyst materials for water splitting, complex oxides of tantalum and niobium have received considerable attention [1–6]. The wide band gap of most niobates and tantalates limits their use to ultraviolet light. However, the favourable location of their conduction bands allows hydrogen evolution from pure water without the need for an applied bias for certain compounds, and they have the added advantage of being very stable against photocorrosion.

The photoelectrochemical activities of niobates and tantalates are indirectly dependent on their crystal structures via the structural influence on the electronic energy levels. For example, the photocatalytic activity for water splitting of $Sr_2Ta_2O_7$ is an order-of-magnitude higher than that for $Sr_2Nb_2O_7$, despite the latter phase having a narrower band gap and thus having access to a wider spectrum of photon energies [1]. The two phases have similar layered perovskite structures [7,8] but the narrower dispersion of bond angles in the corner-connected octahedra in $Sr_2Ta_2O_7$ [1] is considered to be favourable to energy band formation and delocalisation of the electrons with concommittant lower charge recombination. On the other hand, the dipole moments present in the non-centrosymmetric $Sr_2Nb_2O_7$ are considered to be favourable for improving charge separation [1]. Another example of the influence of crystal structure on photocatalytic activity is provided by the compounds R_3NbO_7 and R_3TaO_7, R = rare earth elements. The change in crystal structure, from pyrochlore type to weberite type, as the size of the REE is increased results in an increase in hydrogen evolution by a factor of ~40 [5]. Clearly, there is a subtle interplay between the structure details and the photoactivity for these materials, necessitating careful structure determinations to analyse the structure–property relationships.

*Corresponding author. Fax: +61 3 9562 8919.
E-mail address: ian.grey@csiro.au (I.E. Grey).

0022-4596/$ - see front matter © 2007 Elsevier Inc. All rights reserved.
doi:10.1016/j.jssc.2007.06.014

The tantalate $BaTa_2O_6$ occurs as three different structural polymorphs, with orthorhombic, tetragonal and hexagonal unit cells [9]. The three phases all have a short 3.9 Å projection axis (or 2×3.9 Å for the orthorhombic phase), and their structures can be described in terms of layers of corner- and edge-connected TaO_6 octahedra with Ba atoms occupying different types of tunnels parallel to the short axis [4]. Kato and Kudo [4] have reported that the three phases have quite different photocatalytic activities for water splitting. Recently the high-temperature hexagonal phase has been prepared metastably at low temperature in the form of nanorods by a hydrothermal route and has been shown to have a high photocatalytic activity towards degradation of rhodamine B [6]. However, the crystallographic details needed to interpret the variation of photocatalytic behaviour with structure are not available. A model for the structure of hexagonal $BaTa_2O_6$ ($a_h = 21.14$ Å, $c_h = 3.917$ Å) was proposed by Layden in 1968 [10]. The model was consistent with powder X-ray diffraction (XRD) data, but no refinement of the structure was attempted.

The corresponding hexagonal niobate phase does not form at the stoichiometric 1:1 $BaO:Nb_2O_5$ composition [11]. Instead, a non-stoichiometric phase with a unit cell similar to that for hexagonal $BaTa_2O_6$ was found to occur at approximately 53.5 mol% Nb_2O_5 [12]. A recent phase equilibria study, involving the analysis of a number of closely spaced compositions between 50 and 55 mol% Nb_2O_5, has reported that the phase occurs as a point compound in the $BaO–Nb_2O_5$ system at 52.5 mol% Nb_2O_5 [13]. The close match of the powder pattern with that calculated from the published structure for $BaTa_2O_6$ [10] suggested that the two compounds are isostructural.

In this study, we report the results of refinements of the structures of hexagonal $BaTa_2O_6$ and the non-stoichiometric hexagonal barium niobate using single-crystal XRD data.

2. Experimental

2.1. Crystal growth

$BaTa_2O_6$ crystals were grown using a vanadate flux ($BaO:V_2O_5 = 51:49$ M, m.p. ~710 °C, prepared by melting a mixture of $BaCO_3$ and V_2O_5). Crystals were grown from a mixture of 0.8 g flux and 0.2 g pre-reacted (1550 °C, 16 h) 51:49 (molar) $BaO:Ta_2O_5$ powder. The mixture was heated in an unsealed Pt capsule (3 mm O.D., 2.6 mm I.D., 25 mm L) at 1400 °C for 2 h, followed by slow-cooling at 6 °C/h to 700 °C, and then removal from the furnace. After washing in dilute (2 M) HCl, many crystals of different shapes were obtained. Crystals corresponding to all three polymorphs of $BaTa_2O_6$, as well as $Ba_5Ta_4O_{15}$, were found in this preparation and were easily differentiated by their shapes, mainly controlled by their different crystal structures. Colourless needle-like crystals of hexagonal $BaTa_2O_6$ with the long axis parallel to c_h were harvested for further study.

Colourless tabular crystals of the hexagonal barium niobate analog were obtained from an off-stoichiometric partial melt. Pre-equilibrated (@ 1275 °C) $BaO:Nb_2O_5$ powder of molar composition 41.9:58.1 was heated in an unsealed Pt capsule at 1325 °C for 24 h, slow cooled at 1 °C/h to 1290 °C, and then removed from the furnace. Crystals were harvested mechanically, and checked for quality and purity using the precession method.

2.2. Single-crystal intensity data collections

An acicular crystal of $BaTa_2O_6$ measuring 0.03 mm in diameter and over 0.2 mm long was trimmed with a scalpel to reduce its length to 0.1 mm. Intensity data were collected at room temperature using a Bruker APEX II Kappa CCD diffractometer. The data collection and processing conditions are summarised in Table 1.

Table 1
Summary of data collection conditions and refinement parameters

Formula	$BaTa_2O_6$	$Ba_{0.93}Nb_{2.03}O_6$
Crystal data		
Cell parameters (Å)	$a = 21.116(1)$ $c = 3.9157(2)$	$a = 21.0174(3)$ $c = 3.9732(1)$
Z	12	12
ρ (g/cm^3)	7.84	5.36
Space group	*P6/mmm*	*P6/mmm*
Data collect		
Diffractometer	Bruker APEX II CCD	Bruker APEX II CCD
λ (Mo$K\alpha$)	0.71073	0.71073
Temperature (K)	293	293
Crystal size (mm)	$0.03 \times 0.03 \times 0.10$	$0.08 \times 0.12 \times 0.14$
Collection mode	ϕ scan, 0–360°, $\Delta\phi = 0.5°$ plus ω scans	ϕ scan, 0–360°, $\Delta\phi = 0.5°$ plus ω scans
Count time per frame (s)	50	20
$2\theta_{max}$ (°)	70	70
Reflection range	$-34 \leqslant h,k \leqslant 34$; $-6 \leqslant l \leqslant 5$	$-33 \leqslant h,k \leqslant 33$; $-6 \leqslant l \leqslant 6$
Total no. of reflections	51389	30154
Data completeness (%)	96.1	97.0
No. of unique reflections	1329	1345
No. of reflections, $F > 4\sigma(F)$	1319	1343
Absorption correction (Multi-scan)	$\mu = 51.0$ mm^{-1} $T_{min}/T_{max} = 0.39$	$\mu = 11.4$ mm^{-1} $T_{min}/T_{max} = 0.69$
R_{merg} on F^2	0.052	0.036
Refinement		
No. parameters refined	90	91
R_1, $F > 4\sigma(F)$	0.028	0.047
R_1, all data	0.028	0.047
w$R_2(F^2)$[a], all data	0.056	0.098
GOF	1.03	1.19
Extinction coefficient	0.00064(2)	0.0070(3)

[a] $w = 1/[\sigma^2(F_0^2) + (aP^2 + bP]$, $P = [2F_c^2 + \mathrm{Max}(F_0^2, 0)]/3$ from Ref. [15].

A columnar crystal of hexagonal barium niobate measuring ~0.1 mm in diameter and 0.2 mm long was trimmed using a scalpel to obtain a more equi-dimensional crystal to minimise absorption effects. An intensity data set was collected at room temperature using the Bruker APEX II Kappa CCD diffractometer. The data collection and processing parameters are given in Table 1. The CCD intensity data sets for both crystals were processed and refined using the WinGX program system [14]. SHELX-97 [15] was used within WinGX for the refinements.

2.3. Refinement of hexagonal $BaTa_2O_6$

The atomic coordinates published by Layden [10] in space group $P6/mmm$ were used as starting values for the refinement. The positions and displacement parameters refined satisfactorily for all atoms except Ba(1) at (0,0,0.5) and Ba(3) at (0.5,0,0). The Ba(3) site was found to be split, at (x,0,0), $x = 0.456$, resulting in pairs of half-occupied sites separated by 1.8 Å. There was no electron density for the Ba(1) site at (0,0,0.5). Instead difference Fourier maps showed peaks located near (0,0,0.25) and (0,0,0.1), and Ba(1) atoms were located at these two sites. Refinement with isotropic displacement parameters reduced the R_1 agreement index to 0.079. Refinement with anisotropic displacement parameters first for the metal atoms and then for the oxygen atoms resulted in convergence at $R_1 = 0.028$ for all data. Other refinement details are given in Table 1. The final refined coordinates and equivalent isotropic displacement parameters are given in Table 2.

Table 2
Atomic coordinates ($\times 10^4$) and equivalent isotropic displacement parameters (Å$^2 \times 10^3$) for $BaTa_2O_6$

Atom	Site	x	y	z	U(eq)
Ba(1A)	2*e*	0	0	2760(20)	19(2)
Ba(1B)	12*n*	230	230	820(120)	80(30)
Ba(2)	2*c*	3333	6667	0	33(1)
Ba(3)	6*j*	4563(1)	0	0	10(1)
Ba(4)	6*l*	1838(1)	3676(1)	0	25(1)
Ta(1)	6*m*	1010(1)	2019(1)	5000	11(1)
Ta(2)	6*k*	3069(1)	0	5000	7(1)
Ta(3)	12*q*	5075(1)	1630(1)	5000	6(1)
O(1)	6*k*	1246(5)	0	5000	19(2)
O(2)	12*q*	2830(4)	774(4)	5000	15(1)
O(3)	12*q*	4111(4)	794(4)	5000	32(2)
O(4)	6*m*	4529(2)	9058(5)	5000	9(2)
O(5)	6*m*	3841(2)	7683(5)	5000	15(2)
O(6)	6*m*	2388(3)	4775(5)	5000	13(2)
O(7)	6*l*	1050(4)	2101(9)	0	35(3)
O(8)	6*j*	3093(7)	0	0	45(5)
O(9)	12*p*	5065(6)	1682(6)	0	30(2)

U(eq) is defined as one-third of the trace of the orthogonalised U_{ij} tensor.Fractional site occupancies: Ba(1A) 0.24(1), Ba(1B) 0.029(3), Ba(3) 0.5, other atoms 1.

2.4. Refinement of hexagonal $Ba_{0.93}Nb_{2.03}O_6$

The non-stoichiometric hexagonal barium niobate was also refined in $P6/mmm$ using Layden's coordinates [10] as starting values. As in the case of the tantalate, the Ba(1) and Ba(3) atoms had to be re-located to lower symmetry sites. Isotropic refinement converged at $R_1 = 0.17$. The major peaks in the difference Fourier map corresponded to split Nb(1) to Nb(3) atom sites due to displacement of these atoms by ~0.2 Å along [0 0 1] from the mirror plane at $z = 0.5$. Following relocation of the niobium atoms to sites displaced away from the mirror plane, refinement with isotropic displacement parameters reduced R_1 to 0.13. The strongest peak in the difference Fourier map was located at (0.2,0,0), corresponding to the partial occupation of a tri-capped trigonal prismatic site. Nb was included in this latter site. Refinement of the site occupation factors for the other Nb and Ba atoms showed that only Ba(4) had a significantly reduced occupation factor. Refinement using anisotropic displacement parameters, first for the metal atoms then for all atoms, resulted in convergence at a final R_1 value of 0.047 for all reflections.

The displacement of the niobium atoms away from the mirror plane at $z = 0.5$ in $P6/mmm$ suggested that the niobate may be ferroelectric. Attempts were made to refine ferroelectric models in non-centrosymmetric subgroups of $P6/mmm$ but without success. Equal occupation of niobium sites symmetrical about $z = 0.5$ was obtained. Other refinement details for the $P6/mmm$ refinement are given in Table 1. The final refined coordinates and equivalent isotropic displacement parameters are given in Table 3. Polyhedral bond lengths for both compounds are given in Table 4.

Table 3
Atomic coordinates ($\times 10^4$) and equivalent isotropic displacement parameters (Å$^2 \times 10^3$) for $Ba_{0.93}Nb_{2.03}O_6$

Atom	Site	x	y	z	U(eq)
Ba(1A)	2*e*	0	0	2630(40)	27(4)
Ba(1B)	12*n*	200	200	640(60)	28(9)
Ba(2)	2*c*	3333	6667	0	30(1)
Ba(3)	6*j*	4578(1)	0	0	11(1)
Ba(4)	6*l*	1842(1)	3684(1)	0	22(1)
Nb(1)	12*o*	1010(1)	2020(1)	4544(5)	9(1)
Nb(2)	12*n*	3075(1)	0	4558(6)	7(1)
Nb(3)	24*r*	5076(1)	1629(1)	4580(5)	6(1)
Nb(4)	6*j*	2038(7)	0	0	10(4)
O(1)	6*k*	1251(5)	0	5000	39(3)
O(2)	12*q*	2814(3)	764(3)	5000	24(2)
O(3)	12*q*	4111(4)	792(4)	5000	33(2)
O(4)	6*m*	4535(2)	9069(4)	5000	6(1)
O(5)	6*m*	3836(2)	7672(4)	5000	15(2)
O(6)	6*m*	2386(2)	4771(5)	5000	13(1)
O(7)	6*l*	1040(4)	2080(8)	0	39(3)
O(8)	6*j*	3098(7)	0	0	52(4)
O(9)	12*p*	5059(5)	1661(5)	0	33(2)

U(eq) is defined as one-third of the trace of the orthogonalised U_{ij} tensor.Site occupation fractions: Ba(1A) 0.19(1), Ba(1B) 0.026(2), Ba(3) 0.5, Ba(4) 0.880(5), Nb(1)–Nb(3) 0.5, Nb(4) 0.056(6), other atoms 1.

Table 4
Bond lengths (Å) in $BaTa_2O_6$ and $Ba_{0.93}Nb_{2.03}O_6$

	$BaTa_2O_6$	$Ba_{0.93}Nb_{2.03}O_6$
Ba(1A)–O(1) × 6	2.77(1)	2.79(2)
Ba(1B)–O(1) × 9	2.70(6)–3.52(7)	2.81(6)–3.51(6)
Ba(1B)–O(7) × 2	3.44(5)	3.44(5)
Ba(2)–O(5) × 6	2.699(6)	2.701(5)
Ba(2)–O(9) × 6	3.44(1)	3.45(1)
Ba(3)–O(3) × 4	3.026(6)	3.053(6)
Ba(3)–O(4) × 4	2.766(6)	2.757(4)
Ba(3)–O(8)	3.10(2)	3.11(1)
Ba(3)–O(9) × 2	3.16(1)	3.111(9)
Ba(4)–O(2) × 4	2.838(5)	2.878(5)
Ba(4)–O(6) × 2	2.807(7)	2.803(6)
Ba(4)–O(7)	2.88(2)	2.92(2)
Ba(4)–O(9) × 2	3.110(9)	3.097(7)
Ta/Nb(1)–O(1) × 2	1.931(3)	1.929(3)
Ta/Nb(1)–O(2) × 2	2.007(7)	1.987(6)
Ta/Nb(1)–O(7)	1.964(2)	1.809(1)
Ta/Nb(1)–O(7)	1.964(2)	2.171(2)
Ta/Nb(2)–O(2) × 2	1.937(6)	1.947(6)
Ta/Nb(2)–O(3) × 2	1.991(8)	1.980(6)
Ta/Nb(2)–O(8)	1.959(1)	1.812(2)
Ta/Nb(2)–O(8	1.959(1)	2.163(2)
Ta/Nb(3)–O(3)	1.914(8)	1.914(6)
Ta/Nb(3)–O(4)	2.006(6)	2.013(4)
Ta/Nb(3)–O(5)	2.006(6)	2.015(5)
Ta/Nb(3)–O(6)	1.994(3)	1.996(2)
Ta/Nb(3)–O(9)	1.962(1)	1.822(2)
Ta/Nb(3)–O(9)	1.962(1)	2.155(2)
Nb(4)–O(1) × 2		2.59(1)
Nb((4)–O(2) × 4		2.563(6)
Nb(4)–O(7) × 2		2.143(7)
Nb(4)–O(8)		2.23(2)

3. Results and discussion

3.1. Description of structures

A polyhedral representation of the octahedral framework common to hexagonal $BaTa_2O_6$ and $Ba_{0.93}Nb_{2.03}O_6$ is shown in projection along [0 0 1] in Fig. 1. The Ba atoms are represented by the filled circles in Fig. 1. Individual and edge-shared pairs of MO_6 octahedra (M = Nb or Ta) are connected together by corner-sharing into a relatively complex hexagonal framework that encompasses [0 0 1] channels of five different types, characterised by their shape and the number of octahedral edges that frame them. They include 3-member and 6-member triangular channels, 6-member channels with rectangular (2 × 1) and hexagonal outlines and pentagonal channels. The hexagonal channels are centred on the unit-cell origins and are formed from six $M(1)O_6$ octahedra, corner-connecting via O(1), see Fig. 1. The Ba atoms Ba(1A) and Ba(1B) are located in these channels. The $M(1)O_6$ octahedra are also corner-connected (via O(2), see Fig. 1) with $M(2)O_6$ octahedra, forming six 3-member triangular channels in a concentric arrangement around the hexagonal channels, as in hexagonal tungsten bronze (HTB) structures.

The $M(2)O_6$ octahedra are further corner-linked, via O(3), with edge-shared pairs of octahedra containing $M(3)$. The

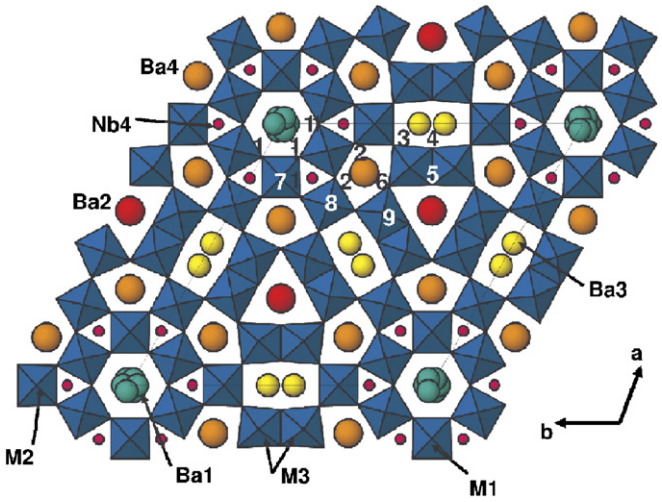

Fig. 1. Polyhedral representation of the structure of BaM_2O_6 projected along [0 0 1]. The labels 1–9 correspond to the oxygen atom labels given in Tables 2 and 3.

$M(2)O_6$ and $M(3)_2O_{10}$ units enclose 2 × 1 rectangular channels, that are occupied by Ba(3). This arrangement of corner- and edge-linked octahedra is topologically identical to the octahedral connectivity in orthorhombic $CaTa_2O_6$ [16] and $SrTa_2O_6$ [17], as well as in the low temperature, monoclinic form of $BaNb_2O_6$ [18]. In these latter compounds however, rotation of the octahedral framework at the flexible corner connections gives channels of elongated hexagonal shape, rather than the near-rectangular channels shown in Fig. 1.

Along each of the equivalent ⟨1 0 0⟩ directions in hexagonal $BaTa_2O_6$ and $Ba_{0.93}Nb_{2.03}O_6$, there is a 1:1 alternation of the above-described elements of HTB and orthorhombic $CaTa_2O_6$ structures. This results in slabs of alternating HTB and *ortho*-$CaTa_2O_6$ structures parallel to the three {1 0 0} planes (≡three-fold twinning of a unit-cell intergrowth of HTB and *ortho*-$CaTa_2O_6$-type structures). The 6-membered triangular channels and the pentagonal channels occur at the interfaces between the three orientations of the {1 0 0} slabs of alternating HTB and *ortho*-$CaTa_2O_6$ elements. The triangular channels derive from the corner-connection of $M(3)_2O_{10}$ edge-shared dimers from three different orientations of the *ortho*-$CaTa_2O_6$ elements, while the pentagonal channels derive from the connection of two different orientations of the *ortho*-$CaTa_2O_6$ elements with an HTB element from a third orientation. Ba(2) and Ba(4) fully occupy sites in the centres of the triangular and pentagonal channels, respectively.

In both $BaTa_2O_6$ and $Ba_{0.93}Nb_{2.03}O_6$, the barium atoms are disordered in the hexagonal and 2 × 1 rectangular channels. Barium atoms partially occupy two different positions in the hexagonal channels as shown in Fig. 2. The major occupied site, Ba(1A), is located close to (0,0,1/4) and a barium atom in this site bonds to a six O(1) atoms at a separation of ~2.8 Å. The next nearest oxygen atoms are O(7) at ~3.9 Å away. The other occupied barium site in the hexagonal channels, Ba(1B), is a multiply split site distributed around (0,0,0). A barium atom located at the

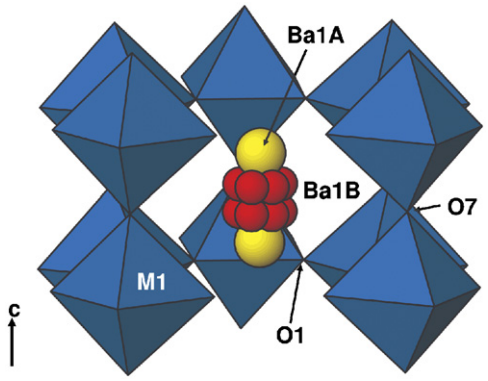

Fig. 2. Location of the disordered barium atoms Ba(1A) and Ba(1B) in the hexagonal cross-section channels. The front octahedron of each of the surrounding hexagonal rings of $M(1)O_6$ octahedra has been removed to show the barium atoms.

origin would have 12 long bonds of 3.3 Å to O(1) and six much longer bonds of 3.9 Å to O(7). By displacing from the origin by ~0.6 Å Ba(1B) is able to achieve some shorter bond distances as shown in Table 4.

In the rectangular channels, the Ba(3) atoms statistically half-occupy two sites on either side of the channel centre, separated by 1.8 Å. Similar off-centre location of the large cations in the 2×1 channels is reported for *ortho*-$CaTa_2O_6$ [16] and $SrTa_2O_6$ [17]. However, in these compounds, the axis defining the channel repeat distance is doubled, allowing for full occupancy of the sites in alternating fashion, giving zig-zag chains of barium atoms along the channels. In hexagonal $BaTa_2O_6$ and $Ba_{0.93}Nb_{2.03}O_6$, with a 3.9 Å projection axis, it is likely that the split Ba(3) positions also correspond locally to zig-zag chains, but with no correlation between adjacent chains. This lateral displacement of the Ba(3) atoms in the 2×1 channels allows the Ba(3)–Ba(3) separation to increase from the *c*-axis repeat distance (<4 Å for both structures) to 4.3 Å.

3.2. Comparison of crystal chemistry of $BaTa_2O_6$ and $Ba_{0.93}Nb_{2.03}O_6$

The structure analyses show that the compositional differences between the isostructural hexagonal tantalate and niobate compounds are due to the niobate having vacancies in the Ba(4) site in the pentagonal channels, as well as having niobium atoms partially occupying interstitial sites in the 3-member triangular channels, which are empty in the tantalate. Both the niobate and the tantalate also have a small shortfall in the occupancy of the hexagonal channel sites by barium. However, the sum of the refined occupancies of Ba(1A) and Ba(1B) is within three e.s.d.s of full occupancy for the tantalate. The apparent shortfall is most likely due to the difficulty of modelling the disorder involving multiply split sites, shown in Fig. 2. On this basis, the composition of the tantalate compound is considered to be stoichiometric $BaTa_2O_6$. For the niobate, the Nb(4) and Ba(4) refined site occupation factors can be used to calculate the composition as $Ba_{0.93}Nb_{2.03}O_6$. This corresponds to a molar composition of 47.8% BaO and 52.2% Nb_2O_5, which is very close to the composition of 47.5% BaO and 52.5% Nb_2O_5 obtained from a recent phase equilibria study [13].

The extra niobium atoms, Nb(4), in $Ba_{0.93}Nb_{2.03}O_6$ occupy interstitial sites with tri-capped trigonal prismatic coordination in the triangular channels. The location of Nb(4) is shown in Fig. 1 and in more detail in Fig. 3. The $Nb(4)O_9$ coordination involves three relatively short bonds, 2.14 and 2.23 Å ($\times 2$) to O(7) and O(8), respectively, in the same (001) plane as Nb(4) and six considerably longer bonds to the trigonal prism corners, occupied by O(1) and O(2), at distances of 2.59 and 2.56 Å, respectively. Similar Nb–O bond distances have been reported for tri-capped trigonal prismatically co-ordinated niobium atoms in other niobates such as the low temperature (*T*) form of Nb_2O_5 [19] and $K_6Nb_{10.8}O_{30}$ [20]. In each case, the 9-coordinated sites are only partially occupied (4–8% in *T*-Nb_2O_5 and $Ba_{0.93}Nb_{2.03}O_6$ and 20% in $K_6Nb_{10.8}O_{30}$). It is likely that at these low concentrations of interstitial atoms, the structure is able to adapt to their bonding requirements by localised displacements of the coordinating oxygen atoms. Because they involve the displacements of only a small fraction of the oxygen atoms, such displacements are unlikely to be resolved from XRD coordinate refinements.

In addition to the stoichiometry difference, the hexagonal barium niobate differs from the hexagonal tantalate in having displacements of the octahedral cations along [0 0 1]. The magnitude of the displacements from the mirror plane at $z = 0.5$ for Nb(1)–Nb(3) are in the range 0.17–0.18 Å. Such displacements are common in ferroelectric niobates with the related tetragonal tungsten bronze (TTB) structure [21] and the polar direction has been reported to be along [0 0 1] in the TTB phases of composition $Ba_{1-x}Sr_xNb_2O_6$ [22].

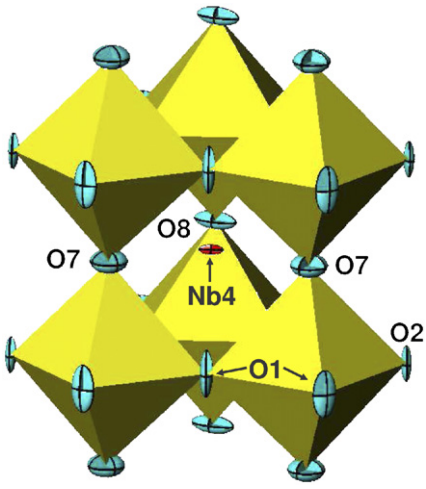

Fig. 3. The coordination environment around Nb(4) in $Ba_{0.93}Nb_{2.03}O_6$. Anisotropic displacement ellipsoids are shown for Nb(4) and the oxygen atoms.

Why does not the niobate form a stoichiometric BaM_2O_6 hexagonal phase like the tantalate? A possible reason is the instability associated with full occupation by barium of the pentagonal channels, which represent 50% of the channel sites in the hexagonal phase. An indication of this instability for the niobate is that the TTB structure, in which pentagonal channels are the dominant sites (60%) for large-cation incorporation, is a stable polymorph for $BaTa_2O_6$ but not for $BaNb_2O_6$ [23]. However, stable TTB niobate structures can be formed by partial substitution of a smaller A cation for Ba, e.g. $Ba_{1-x}Sr_xNb_2O_6$ [22], by partial reduction of niobium to expand the framework as in $Ba_3Nb_5O_{15}$ [24] (note that this is the composition for TTB with both pentagonal and square section channels fully occupied), or by reducing the concentration of Ba in the channels by decreasing the Ba/Nb ratio [13]. These observations all suggest that full occupancy of the pentagonal channels by Ba produces high local stresses.

One of the causes of such stresses is the close approach of niobium atoms Nb(1) and Nb(3) to Ba(4) which constrain the barium atom through non-bonded cation–cation repulsions. The structural environment around the Ba(4) site is shown in Fig. 4. The niobium atoms form a trigonal prismatic cage about Ba(4) with Ba(4)–Nb(1) = 3.63 Å (× 2) and Ba(4)–Nb(3) = 3.75 Å (× 4), whereas the Nb(2) atoms are almost 4 Å away. The scope for displacement of Ba(4) towards the Nb(2) atoms is limited, however, by the consequent lengthening of the shorter Ba(4)–O bonds. This in turn limits the ability of the Ba(4) atoms to reduce their strong Ba–Ba non-bonded repulsions along the channel axis by polarising to flatten the electron shell along [0 0 1]. In contrast to the constraints on Ba(4), the other Ba atoms in the hexagonal BaM_2O_6 structure are able to ease strong non-bonded Ba–Ba repulsions, by either large lateral displacements in the channels to give lengthened zig-zag chains along [0 0 1] (Ba(3)), by displacement and disorder (Ba(1)), or by contracting in size through forming strong bonds to oxygens (Ba(2)–O(5)).

In hexagonal $Ba_{0.93}Nb_{2.03}O_6$, the strong Ba(4)–Ba(4) non-bonded repulsions are relieved by having vacancies at the Ba(4) site, towards which adjacent barium atoms can relax. The deficiency in positive charge is balanced by extra niobium atoms occupying the tri-capped trigonal prismatic site Nb(4). Niobium in this interstitial site has short Nb–Nb distances of 2.93 to 2.94 Å to the six surrounding Nb(1) and Nb(2) atoms, and the associated Nb(4)–O(7,8)–Nb(1,2) angles are close to 90°. Blasse [25] has described how this type of right-angled *M*–O–*M* configuration is particularly favoured in niobate compounds and can lead to stability through electron delocalisation from oxygen to empty *d*-orbitals on the niobium and formation of niobium ion-niobium ion bonds. Blasse [25] also commented that such an arrangement is not favourable for tantalates because of the greater ionic character of the Ta–O bonds. Thus, in $Ba_{0.93}Nb_{2.03}O_6$ there is a synergy between the formation of barium vacancies and the maintaining of charge balance by incorporation of Nb at interstitial sites, which is not expected to occur for the tantalate.

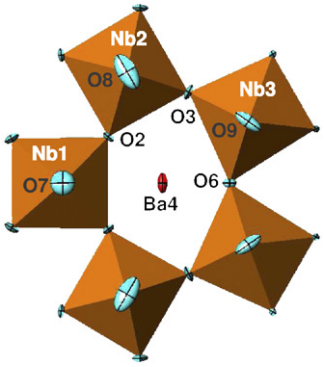

Fig. 4. The coordination environment around Ba(4) in $Ba_{0.93}Nb_{2.03}O_6$. Anisotropic displacement ellipsoids are shown for Ba(4) and the oxygen atoms.

How does the tantalate accommodate the potential instability of the non-bonded Ba(4)–Ba(4) repulsions in the pentagonal channels? A possible clue is that hexagonal $BaTa_2O_6$ is only stable at high temperatures, above 1300 °C [9]. The TTB form of $BaTa_2O_6$ with similar occupied pentagonal channels is also a high-temperature phase, stable in the narrow temperature range 1150–1300 °C [9]. Expansion of the structures at these high temperatures will tend to relieve the repulsive forces. An important aspect that is not often considered in discussions of structure stability is the vibrational free energy contribution to the overall free energy. When comparing the relative stabilities of isostructural niobate and tantalate phases at elevated temperatures, account needs to be taken of the larger atomic mass of Ta compared to Nb. The Ta–O vibrations occur at lower frequencies than Nb–O vibrations and these lower frequency contributions to the phonon density of states will give a more negative vibrational free energy for the tantalate compared with the niobate. The total energy of the tantalate will then be lower than that of the niobate even if the two structures are otherwise identical (same bond lengths). The increasing contribution of the vibrational entropy component, $T\Delta S^{vib}$, with increasing temperature may then stabilise a phase such as $BaTa_2O_6$ in the hexagonal form at high temperatures where the corresponding niobate, with a lower ΔS^{vib} contribution, remains unstable relative to other structure forms or combinations of phases. In the case of $BaNb_2O_6$, the stoichiometric hexagonal phase is unstable relative to the *ortho*-$CaTa_2O_6$-type phase [16,18] at low temperatures and to a unit-cell-twinned form [17] of the $CaTa_2O_6$ structure at temperatures above ~1200 °C. These two structures are illustrated in Figs. 5(a) and (b), respectively.

3.3. Related structures

The only other reported hexagonal-$BaTa_2O_6$-type structure to our knowledge is that for $K_{0.305}Ba_{0.695}Nb_{2.03}O_6$ [26]. This phase has the same concentration of excess

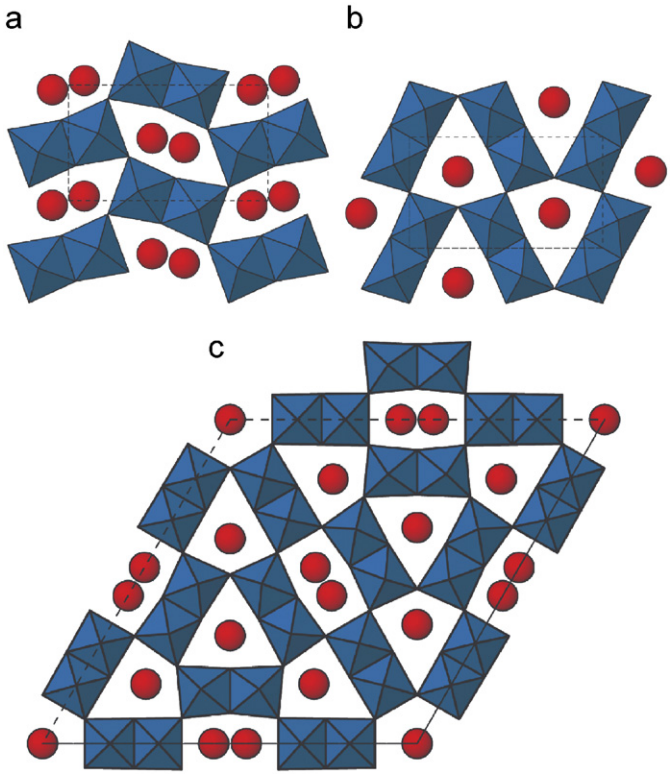

Fig. 5. Polyhedral representations, viewed along the channel axes, of the structures of (a) low-temperature $BaNb_2O_6$ with the orthorhombic $CaTa_2O_6$ structure, (b) low-temperature $BaTa_2O_6$, (c) hypothetical structure obtained from hexagonal $BaTa_2O_6$ by a 30 °C rotation of the hexagonal rings of $M(1)O_6$ octahedra. The large cations are shown as filled circles.

niobium atoms in tri-capped trigonal prismatic Nb(4) sites as does $Ba_{0.93}Nb_{2.03}O_6$. The excess niobium atoms provide charge balance for the partial replacement of divalent Ba^{2+} by monovalent K^+. The refinement of the site occupancies in $K_{0.305}Ba_{0.695}Nb_{2.03}O_6$ [26] showed that K was fully ordered in the hexagonal channels at the origin and substituted for 36% of the Ba atoms in the pentagonal channels and for 17% of the Ba atoms in the 2×1 rectangular channels. The structural parameters reported for $K_{0.305}Ba_{0.695}Nb_{2.03}O_6$ [26] are very similar to those obtained for $Ba_{0.93}Nb_{2.03}O_6$, including the coordination of Nb(4) (three bonds in the range 2.15–2.22 Å plus six longer bonds) and the splitting of the Ba/K in the 2×1 rectangular channels, with Ba/K–Ba/K = 1.77 Å.

In Section 3.1, we commented that the hexagonal BaM_2O_6 structure could be described in terms of an intergrowth of *ortho*-$CaTa_2O_6$-type and HTB-type structure elements in slabs parallel to {1 0 0}. The structural relationship of the hexagonal phase to the *ortho*-$CaTa_2O_6$ structure adopted by $BaNb_2O_6$ at low temperature [18] (Fig. 5(a)) and also to the low temperature $BaTa_2O_6$ structure [23] (Fig. 5(b)) becomes apparent from an inspection of the packing of the metal atoms. The metal atom arrangement is the same for the low temperature forms of both $BaNb_2O_6$ and $BaTa_2O_6$ and is shown in projection in Fig. 6(a). It comprises honeycomb layers of

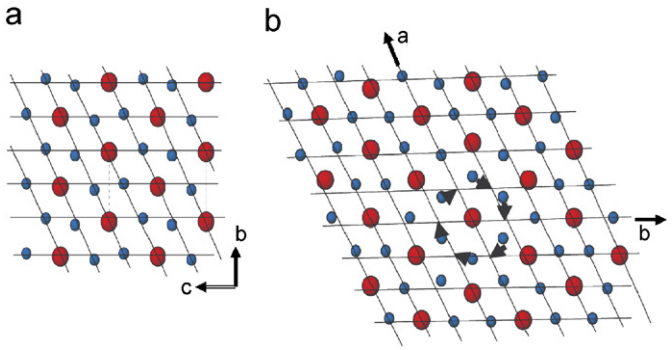

Fig. 6. (a) Array of M atoms (small circles) and Ba atoms (large circles) common to the low-temperature forms of $BaNb_2O_6$ and $BaTa_2O_6$. (b) Array of M and Ba atoms in hexagonal BaM_2O_6. Arrows show the movement of the hexagonal ring of $M(1)$ atoms that transforms the array to that shown in (a).

M atoms, with Ba atoms located between the layers, having a hexagonal ring of M atoms above and below. The projected $M+Ba$ atom positions lie close to a hexagonal lattice as shown by the grid drawn on Fig. 6(a). The corresponding $Ba+M$ array for hexagonal BaM_2O_6 is shown in projection along [0 0 1] in Fig. 6(b) (the Ba(3) atoms are shown as unsplit for simplicity of presentation). The metal atom array in the hexagonal phase can be converted to that shown in Fig. 6(a) by a co-operative rotation by 30° of the six $M(1)$ atoms around the origin. The displacements involved are shown by the arrows in Fig. 6(b).

A polyhedral representation of the hexagonal BaM_2O_6 structure after applying the 30° rotation to the ring of six $M(1)O_6$ octahedra is shown in Fig. 5(c). A comparison of Fig. 5(c) with the hexagonal structure in Fig. 1 shows that the result of the rotation of the $M(1)O_6$ octahedra is to eliminate the 5-M pentagonal and 3-M triangular channels and replace them with 6-M triangular channels. The rotated structure is then composed of elements of the low temperature structures of $BaNb_2O_6$ and $BaTa_2O_6$ as seen by a comparison of Fig. 5(c) with Figs. 5(a) and (b). The hexagonal channels at the origin are maintained in the rotational transformation.

4. Conclusions

$BaTa_2O_6$ forms as a stable phase with a hexagonal structure in the BaO–Ta_2O_5 system above 1300 °C, whereas in the BaO–Nb_2O_5 system the hexagonal phase only forms at the off-stoichiometric composition $Ba_{0.93}Nb_{2.03}O_6$. Both structures have $P6/mmm$ symmetry with $a\approx21.1$ Å, $c\approx3.9$ Å and comprise a framework of corner- and edge-connected octahedra centred on the Nb/Ta atoms, with barium atoms occupying sites in four different types of [0 0 1] channels, with triangular, rectangular, hexagonal and pentagonal cross-sections. Single-crystal structure refinements for both phases confirmed the structure model originally proposed by Layden [10], except for large displacements of the Ba(1) and Ba(3) atoms from the

high-symmetry sites originally proposed. The refinements showed that the non-stoichiometry in the niobate phase is due to barium atom vacancies in the pentagonal channels together with niobium interstitial atoms in tri-capped trigonal prismatic sites. The metal atom array in the hexagonal phase can be transformed to the metal atom arrays present in the low-temperature forms of $BaNb_2O_6$ and $BaTa_2O_6$ by co-operative rotation (by 30°) of the metal atoms comprising the hexagonal rings centred at the unit-cell origin.

References

[1] A. Kudo, H. Kato, S. Nakagawa, J. Phys. Chem. B 104 (2000) 571–575.
[2] J. Ye, Z. Zou, A. Matsushita, Int. J. Hydrogen Energy 28 (2003) 651–655.
[3] Z. Zou, H. Arakawa, J. Photochem. Photobiol. A: Chem. 158 (2003) 145–162.
[4] H. Kato, A. Kudo, Catal. Today 78 (2003) 561–569.
[5] R. Abe, M. Higashi, Z. Zou, K. Sayama, Y. Abe, H. Arakawa, J. Phys. Chem. B Lett. 108 (2004) 811–814.
[6] T. Xu, X. Zhao, Y. Zhu, J. Phys. Chem. B 110 (2006) 25825–25832.
[7] K. Scheunemann, H. Mueller-Buschbaum, J. Inorg. Nucl. Chem. 37 (1975) 1679–1680.
[8] N. Ishizawa, F. Marumo, T. Kawamura, M. Kimura, Acta Crystallogr. B 32 (1976) 2564–2566.
[9] G.K. Layden, Mater. Res. Bull. 2 (1967) 533–539.
[10] G.K. Layden, Mater. Res. Bull. 3 (1968) 349–360.
[11] R.S. Roth, J.L. Waring, J. Res. Natl. Bur. Stand. 65A (1961) 337–344.
[12] J.M. Miller, R.S. Roth, L.D. Ettlinger, H.S. Parker, J. Solid State Chem. 67 (1987) 259–270.
[13] T.A. Vanderah, T.R. Collins, W. Wong-Ng, R.S. Roth, L. Farber, J. Alloys Compds. 346 (2002) 116–128.
[14] L.J. Farrugia, J. Appl. Crystallogr. 32 (1999) 837–838.
[15] G.M. Sheldrick, SHELXL, University of Gottingen, Germany, 1997.
[16] L. Jahnberg, Acta Chem. Scand. 17 (1963) 2548–2559.
[17] V.P. Sirotinkin, S.P. Sirotinkin, Zh. Neorgan. Khim. 38 (1993) 1071–1073.
[18] S.P. Sirotinkin, V.P. Sirotinkin, V.K. Trunov, Zh. Neorgan. Khim. 35 (1990) 1609–1611.
[19] K. Kato, S. Tamura, Acta Crystallogr. B 31 (1975) 673–677.
[20] P. Becker, P. Held, Z. Kristallogr. 215 (2000) 319–320.
[21] J. Ravez, J.-P. Budin, P. Hagenmuller, J. Solid State Chem. 5 (1972) 239–246.
[22] P.B. Jamieson, S.C. Abrahams, J.L. Bernstein, J. Chem. Phys. 48 (1968) 5048–5057.
[23] F. Galasso, G. Layden, G. Ganung, Mater. Res. Bull. 3 (1968) 397–408.
[24] B. Hessen, S.A. Sunshine, T. Siegrist, A.T. Fiory, J.V. Waszczak, Chem. Mater. 3 (1991) 528–534.
[25] G. Blasse, J. Inorg. Nucl. Chem. 26 (1964) 1191–1199.
[26] W. Zhang, N. Kumada, T. Takei, J. Yamanaka, N. Kinomura, Mater. Res. Bull. 40 (2005) 1177–1186.